Electronic Supplementary Material (ESI) for Physical Chemistry Chemical Physics.
This journal is © the Owner Societies 2020

Electronic Supplementary Information

First-principles study of $CaB_{12}H_{12}$ as a potential solid-state conductor for Ca

Julius Koettgen,[a,b,d] Christopher J. Bartel,[b] Jimmy-Xuan Shen,[a,c] Kristin A. Persson,[a,c] Gerbrand Ceder*[a,b]

[a] Materials Sciences Division, Lawrence Berkeley National Laboratory, Berkeley, CA 94720, USA. E-mail: gceder@berkeley.edu

[b] Department of Materials Science and Engineering, University of California, Berkeley, CA 94720, USA

[c] Energy Technologies Area, Lawrence Berkeley National Laboratory, Berkeley, CA 94720, USA.

[d] Present address: Volkswagen AG, Volkswagen Group Components, Salzgitter, Germany.

Structure, stability, and Ca mobility were calculated with density functional theory (DFT)[1] using the Vienna Ab Initio Simulation Package (VASP)[2]. The Generalized Gradient Approximation (GGA) as formulated by Perdew, Burke and Ernzerhof (PBE)[3] and the projector augmented-wave method (PAW)[4] with an energy cut-off of 520 eV for plane waves was applied. 2 x 2 x 2 supercells (e.g., $Ca_{16}B_{192}H_{192}$) and a 1 x 1 x 1 Gamma-centered *k*-point mesh were used for all calculations in agreement with a previous work on $K_3BH_4B_{12}H_{12}$.[5] The positions of the atoms and the cell size were optimized for the pristine structure. Minimum energy pathways were calculated by linearly interpolating seven images between the optimized initial and final structure and subsequently applying the nudged elastic band method (NEB).[6] All minimum energy pathways assume a vacancy hopping mechanism in agreement with literature on $Li_2B_{12}H_{12}$ and $Na_2B_{12}H_{12}$.[7] For the mobility calculations with a Ca vacancy only the positions of the atoms (and not the cell shape or volume) were optimized. Electronic and ionic relaxation were performed with convergence parameters of 10^{-5} eV and below 3 x 10^{-2} eV Å^{-1} (except for the high-energy migration path with a length of 7.15 Å which was only converged to 8 x 10^{-2} eV Å^{-1}), respectively. In the mobility calculations, one Ca vacancy was created and excess electrons were balanced by a neutralizing background charge.[8–10] The Ca-free $B_{12}H_{12}$ framework was calculated by removing the Ca ions and calculating the cell at fixed geometry. For $Ca_{15}B_{192}H_{190}$ and $Ca_{15}B_{190}C_2H_{192}$, the lowest energy structure of five non-symmetry equivalent structures was applied. For $Ca_{13}M_2B_{192}H_{192}$, the lowest energy of four non-symmetry equivalent structures was used (cp. Fig. S3) and minimal structural changes to the host $CaB_{12}H_{12}$ structure were observed. Energies for dopant elements in their elemental state were taken from the lowest energy structures for each element available in the Materials Project database.[11] Similarly, the energies for all competing phases used to evaluate the decomposition reactions shown in Table S1 were taken from the Materials Project database. Figures were created using in-house tools and VESTA.[12] Kinetic Monte Carlo (KMC) simulations were performed using the software MOCASSIN with computational details of the simulation discussed in detail in literature before.[13] 10 x 10 x 10 supercells (Table S2) were randomly doped (with any trivalent dopant, e.g. Al, Bi, or a rare-earth element) according to the doping concentrations given in Fig. S4 and the doping equation given in the manuscript. Two diffusion paths of 0.65 eV (10^{13} Hz) between layers have been considered and 10^6 Monte Carlo steps per particle (MCSP) have been performed at 375 K to indicate how both low percolating migration barriers as well as a sufficient concentration of Ca vacancies influence the Ca ion conductivity. In Fig. S4, the KMC-predicted Ca conductivity is plotted against the doping concentration. It is clear that Ca conductivity increases as Ca vacancies are created by the aliovalent dopant until there are sufficiently many dopant ions that the percolating pathways for Ca diffusion become blocked. Note that these simulations account only for the effect that doping places on the configurations of Ca, Ca vacancies, and doping ion, and cannot account for the role the trivalent ion may play in modifying the structure of the material. However, given the relatively low concentration of dopants required to achieve high conductivity and the high coordination of dopant ions by H, we do not expect the substitution of Ca with trivalent ions to drastically alter the Ca migration pathway.

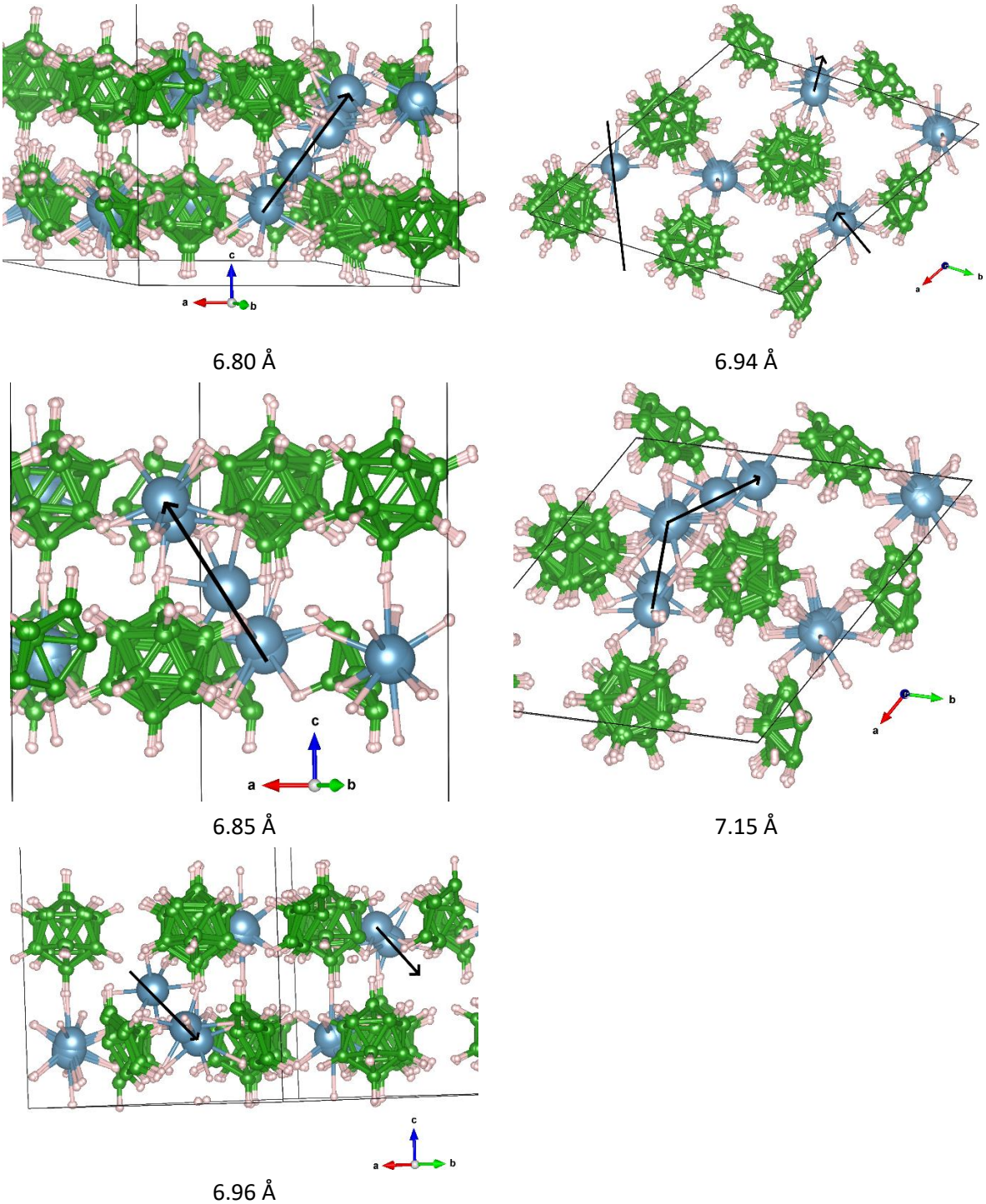

Fig. S1: Ca migration minimum energy paths in $CaB_{12}H_{12}$ calculated by the nudged elastic band calculations. Ca is shown as blue spheres, B as green spheres, and H as grey spheres. An overlay of all calculated images and atom positions along the minimum energy path are shown. The black arrows indicate the migration path of the Ca ions.

The distances between the positions of the migrating Ca show a variation between small and large distances between the NEB images. The reason for this is the additional motion of the surrounding $B_{12}H_{12}$ cages as already discussed in detail before by K. E. Kweon, J. B. Varley, P. Shea, N. Adelstein, P. Mehta, T. W. Heo, T. J. Udovic, V. Stavila and B. C. Wood, Chem. Mater., 2017, 29, 9142–9153. As a

result, a small local minimum can be observed in the energy along the reaction coordinate for the migration path of 7.15 Å (see Fig. 2).

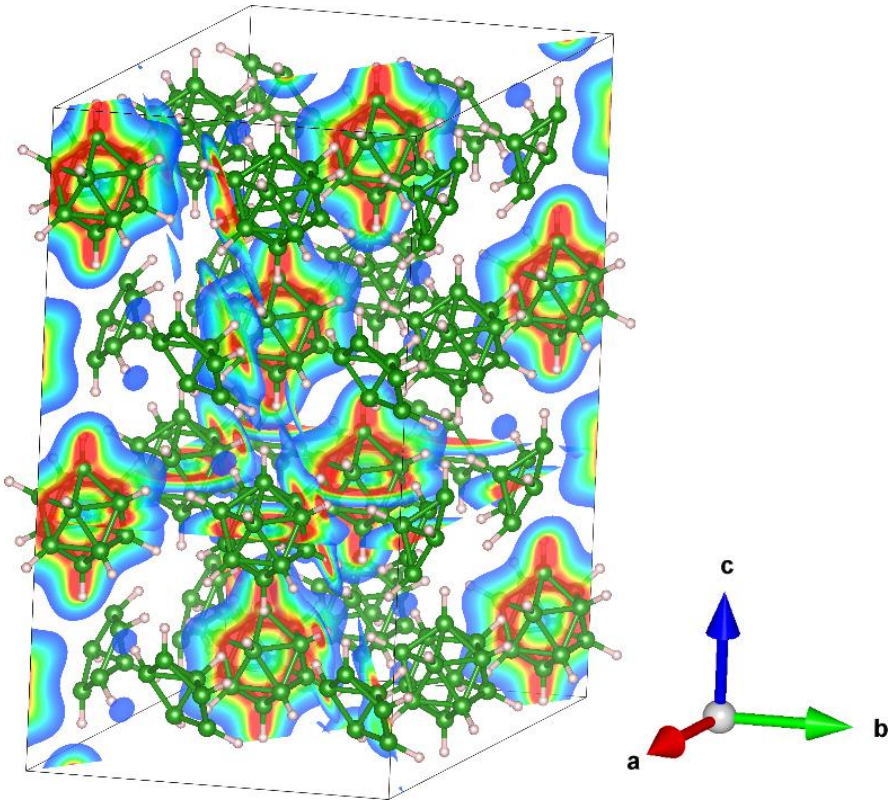

Fig. S2: Structure and charge density of $B_{12}H_{12}$ along all Ca migration paths. Planes and their charge density are shown according to Fig. 3 in the main text. B is shown as green spheres and H as grey spheres.

Table S1: Formation energy, equilibrium reaction energy, and decomposition products for the structure $Ca_{13}M_2B_{192}H_{192}$. Doping $CaB_{12}H_{12}$ with Al, Bi, and rare-earth elements is energetically favorable.

Compound	Formation energy per atom from the elemental references (eV)	Equilibrium reaction energy from the neighbouring equilibrium stable entries (inverse distance to hull) or, for unstable compounds; Energy above hull per atom (eV)	Decomposes to
Ca13La2(BH)192	-0.387	-0.014	Stable
Ca13Ce2(BH)192	-0.384	-0.013	Stable
Ca13Pr2(BH)192	-0.385	-0.015	Stable
Ca13Nd2(BH)192	-0.385	-0.015	Stable
Ca13Pm2(BH)192	-0.384	-0.021	Stable
Ca13Sm2(BH)192	-0.384	-0.014	Stable
Ca13Eu2(BH)192	-0.379	-0.008	Stable
Ca13Gd2(BH)192	-0.384	-0.014	Stable
Ca13Tb2(BH)192	-0.383	-0.013	Stable
Ca13Dy2(BH)192	-0.383	-0.012	Stable
Ca13Ho2(BH)192	-0.382	-0.012	Stable
Ca13Er2(BH)192	-0.382	-0.011	Stable
Ca13Tm2(BH)192	-0.381	-0.011	Stable

Ca13Yb2(BH)192	-0.376	-0.007	Stable
Ca13Lu2(BH)192	-0.384	-0.015	Stable
Ca13(B97H96)2	-0.320	0.036	Ca(BH)12+B9H11+B
Ca13B192(H96N)2	-0.310	0.063	Ca(BH)12+B9H11+B6H10N+B
Ca13Al2(BH)192	-0.364	-0.007	Stable
Ca13B192(PH96)2	-0.350	0.013	B5H7+B2H5+B6P+Ca(BH)12
Ca13B192(H96Cl)2	-0.351	0.014	B9H11+BCl3+Ca(BH)12+B
Ca13Sc2(BH)192	-0.380	-0.012	Stable
Ca13Cr2(BH)192	-0.357	0.007	CrB4+B9H11+Ca(BH)12+CrB
Ca13Fe2(BH)192	-0.345	0.016	FeB2+Ca(BH)12+B9H11+B
Ca13Co2(BH)192	-0.340	0.020	Ca(BH)12+B9H11+CoB+B
Ca13Ga2(BH)192	-0.348	0.008	B9H11+Ca(BH)12+Ga+B
Ca13B192(AsH96)2	-0.344	0.015	B6As+B9H11+Ca(BH)12+As
Ca13B192(H96Br)2	-0.345	0.014	B9H11+Ca(BH)12+BBr3+B
Ca13Y2(BH)192	-0.383	-0.012	Stable
Ca13B192(H96Ru)2	-0.337	0.023	B9H11+B2Ru+Ca(BH)12+B
Ca13B192(H96Rh)2	-0.343	0.017	B9H11+Ca(BH)12+BRh+B
Ca13In2(BH)192	-0.354	0.002	B9H11+Ca(BH)12+In+B
Ca13B192(SbH96)2	-0.353	0.003	B9H11+Ca(BH)12+B+Sb
Ca13B192(H96I)2	-0.347	0.009	B10H13I+B9H11+Ca(BH)12+B
Ca13B192(H96Ir)2	-0.345	0.013	B9H11+BIr+Ca(BH)12+B
Ca13B192(H96Au)2	-0.336	0.020	B9H11+Ca(BH)12+Au+B
Ca13Tl2(BH)192	-0.349	0.016	B9H11+Tl(BH)6+Ca(BH)12+B
Ca13Bi2(BH)192	-0.357	-0.001	Stable

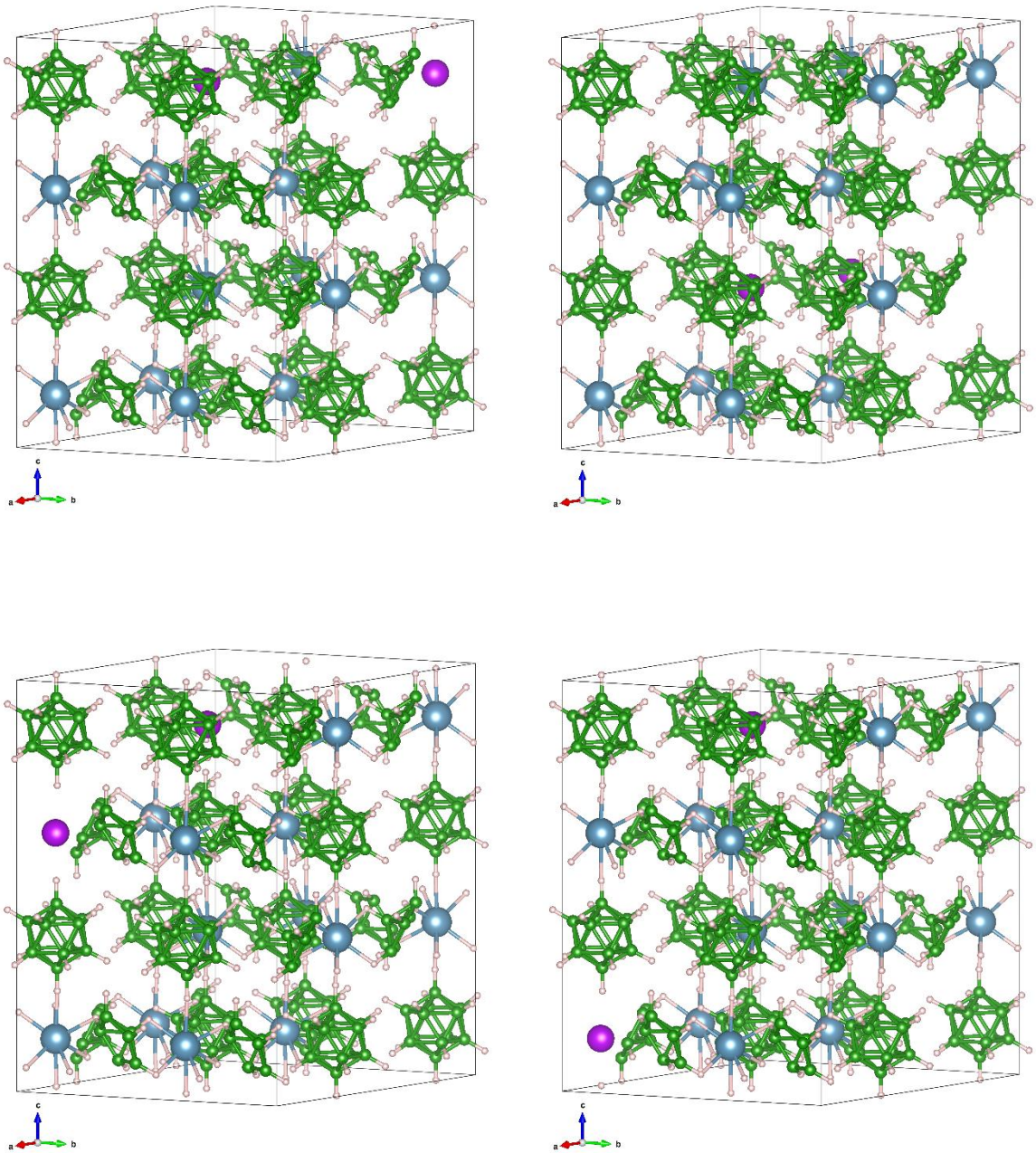

Fig. S3: Considered structures of $Ca_{13}Gd_2B_{192}H_{192}$. Ca is shown as blue spheres, Gd as pink spheres, B as green spheres, and H as grey spheres.

Table S2: Input structure for the kinetic Monte Carlo simulations using a cell with the Space group 15 (C2/c), a = 7.242 Å, b = 11.971 Å, c = 10.744 Å, β = 89.82 ° as given in V. Stavila, J.-H. Her, W. Zhou, S.-J. Hwang, C. Kim, L. A. M. Ottley and T. J. Udovic, J. Solid State Chem., 2010, 183, 1133–1140.

Atoms	x	y	z
Ca	0	0.832	0.25

B1	-0.1721	0.2518	0.3242
B2	-0.1721	0.0992	0.3242
B3	0.0677	0.2989	0.3216
B4	0.0677	0.052	0.3216
B5	0.0032	0.1755	0.4116
B6	0.2159	0.1755	0.3199
H1	-0.2966	0.307	0.3779
H2	-0.2966	0.044	0.3779
H3	0.1167	0.3882	0.3733
H4	0.1167	-0.0372	0.3733
H5	0.0055	0.1755	0.5286
H6	0.3721	0.1755	0.3705
Mig1	0	0.832	0.25
	0.25	0.75	0.5
	0.5	0.668	0.75
Mig2	0.5	0.332	0.25
	0.25	0.25	0.5
	0	0.168	0.75

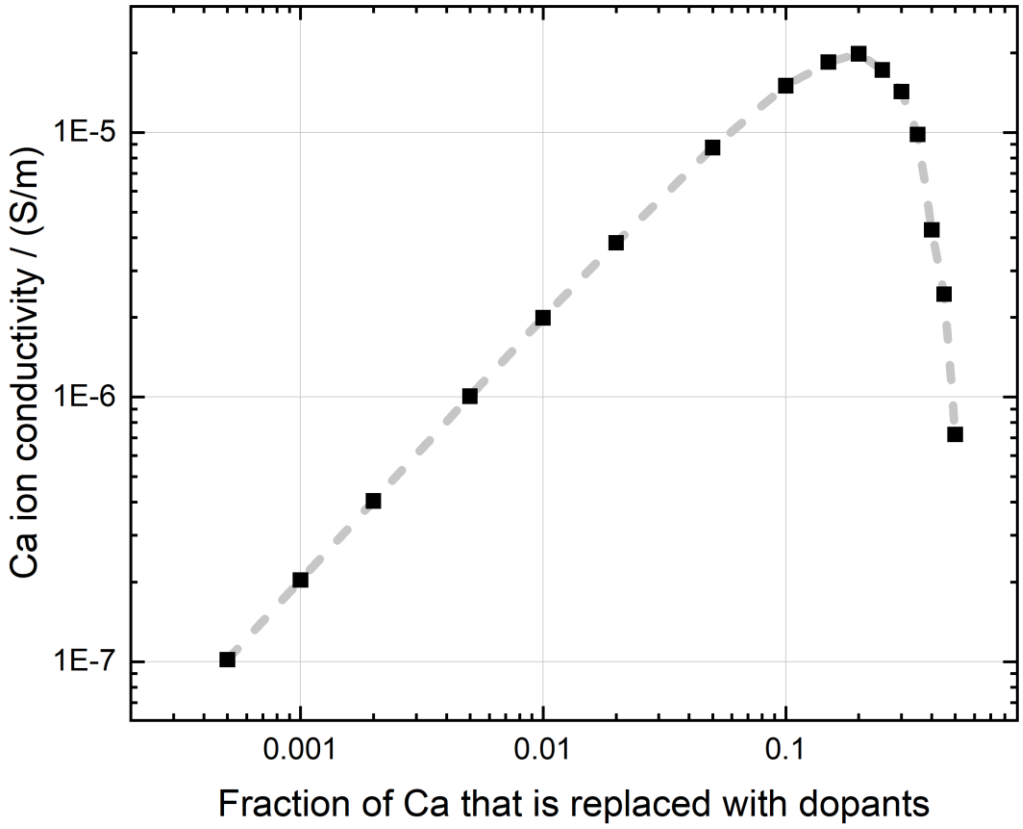

Fig. S4: Kinetic Monte Carlo simulation results show that the Ca ion conductivity increases and subsequently decreases as a function of the fraction of Ca that is replaced by dopants. Doping can increase the Ca ion conductivity by two orders of magnitude.

Notes and references

1 W. Kohn and L. J. Sham, *Phys. Rev.*, 1965, **140**, A1133–A1138.
2 G. Kresse and J. Furthmüller, *Phys. Rev. B*, 1996, **54**, 11169.
3 J. P. Perdew, K. Burke and M. Ernzerhof, *Phys. Rev. Lett.*, 1996, **77**, 3865–3868.
4 G. Kresse and D. Joubert, *Phys Rev B*, 1999, **59**, 1758–1775.
5 Y. Sadikin, R. V. Skoryunov, O. A. Babanova, A. V. Soloninin, Z. Lodziana, M. Brighi, A. V. Skripov and R. Cerny, *J. Phys. Chem. C*, 2017, **121**, 5503–5514.
6 D. Sheppard, R. Terrell and G. Henkelman, *J. Chem. Phys.*, 2008, **128**, 134106.
7 K. E. Kweon, J. B. Varley, P. Shea, N. Adelstein, P. Mehta, T. W. Heo, T. J. Udovic, V. Stavila and B. C. Wood, *Chem. Mater.*, 2017, **29**, 9142–9153.
8 Y. Wang, *Nat Mater*, 2015, **14**, 1026–1031.
9 P. Canepa, S.-H. Bo, G. Sai Gautam, B. Key, W. D. Richards, T. Shi, Y. Tian, Y. Wang, J. Li and G. Ceder, *Nat Commun*, 2017, **8**, 1759.
10 J. Koettgen, P. C. Schmidt, T. Bučko and M. Martin, *Phys Rev B*, 2018, **97**, 024305.
11 A. Jain, S. P. Ong, G. Hautier, W. Chen, W. D. Richards, S. Dacek, S. Cholia, D. Gunter, D. Skinner, G. Ceder and K. A. Persson, *APL Mater.*, 2013, **1**, 011002.
12 K. Momma and F. Izumi, *J. Appl. Crystallogr.*, 2011, **44**, 1272–1276.
13 S. Eisele, S. Grieshammer, *J. Comput. Chem.*, 2020, **31**, 2663–2677.